Sohag Journal of Sciences
An International Journal

Molecular Modeling, Breast Cancer, and Hepatitis A, B, C Molecular Docking Investigation of (2E)-1-phenyl-butane-1,2,3-trione 2-[(2-oxo-2H-chromene-6-yl)hydrazone]

Aly Abdou * *, Hassan M. Mostafa , Abdel-Mawgoud M. Abdel-Mawgoud*

Chemistry Department, Faculty of Science, Sohag University, Sohag 82524, Egypt

Received: 3 Aug. 2022, Revised: 26 Aug. 2022, Accepted: 26 Aug. 2022.
Published online: 1 Sep. 2022

Abstract: Density Functional Theory (DFT) was used to optimize the geometry of (2E)-1-phenyl-butane-1,2,3-trione 2-[(2-oxo-2H-chromene-6-yl)hydrazone]. The DFT computations were based on the B3LYP/6-311G (d, p) level. For the optimized structure, the border molecular orbital, the highest occupied molecular orbital (HOMO), the lowest unoccupied molecular orbital (LUMO), the molecular electrostatic potential (MEP), and a Mulliken population analysis have been done. At the same theoretical level, the vibrational frequencies (FT-IR) of the titled compound were determined and scaled down using a factor of 0.961. Also, at the same level of theory, the electronic spectrum of the mentioned molecule was theoretically estimated using Time-Dependent Density Functional Theory (TD-DFT) in gas phase. The mentioned molecule was subjected to molecular docking investigations to determine its inhibitory activity against the breast cancer receptor (PDB ID: 3I89), the HCV receptor (PDB ID: 5TRH), the HBV receptor (PDB ID: 5T2P), and the HAV receptor (PDB ID: 5WTG). According to the findings, the aforementioned compound has a higher maximum binding affinity for HBV than the others do. Consequently, it might be a good candidate for an antiviral therapy.

Keywords: DFT HOMO; LUMO; MEP; Molecular docking; breast cancer; HCV; HBV; HAV.

1-Introduction

Because of its relatively low cost implications and apparent ease of use, molecular docking has emerged as a key technique in the drug development toolbox, enjoying rising appeal among academic communities. The study of molecular docking involves fitting two or more molecules together, such as a medication and an enzyme or protein. To put it simply, docking is a method of molecular modelling that is used to foretell how an enzyme or protein would interact with tiny molecules (ligands)[i].

The main purpose of molecular docking is to predict how tiny drug-like compounds will bind to their target proteins. Protein misfunction is a common cause of disease, and therapies often rely on blocking or activating the target proteins. Typical lead generation techniques for drug development involve testing a wide range of intriguing compounds against a particular protein that is known to be a disease target in the hopes of detecting a binding relationship [ii]. Similar to experimental high-throughput screening, docking can be used to visually screen new compounds. It also provides atomistic level knowledge to aid in structure-based drug design, where the goal is to identify stable binding conformations between a ligand and a receptor.

It is well known that traditional methods for the development and discovery of new therapeutic agents or drugs involve time-consuming, expensive, and rigorous scientific *in vivo* and *in vitro* processes. As a result, computer-aided *in silico* techniques are increasingly important today for the designing and formulation of new therapeutic agents or drugs to supplement the old traditional method [iii].

Contrarily, the coumarin moiety, one of the many heterocyclic compounds, is a common component of natural products and has distinctive structural characteristics and a broad range of biological activity [iv]. In order to design, formulate, and develop coumarin-based therapeutic agents in a wide range of medical fields, such as anticancer, anti-HIV, antimicrobial, anticonvulsant, antihypertensive, analgesic, anti-inflammatory, antidepressant, analgesic, antileishmanial, anticonvulsant, anti-inflammatory, etc., pharmaceutical industries have taken advantage of the unique structural features of the coumarin moiety [v,vi]. Azo compounds were been found to have high HIV-1 protein inhibiting activity [vii].

Additionally, two FDA-approved medications with azo linkage are prontosil, an antibiotic, and phenazopyridine, a local anaesthetic with effects on urinary tract infections

* Corresponding author E-mail: mohamed2018521500879@gmail.com

[viii]. As a result, the combination of an azo (N=N) moiety and a coumarin ring in a single molecule may lead to the synthesis of substances with unique characteristics [ix]. Therefore, a computational analysis of these azo coumarin derivatives' ability to inhibit hepatitis A, B, C, and breast cancer using molecular docking has been attempted.

2- Materials and method

2.1. Synthesis

The synthetic 6-aminocoumarin [x] was diazotized as usual by dissolving it in hydrochloric acid, bringing the solution to a temperature between 0 and 5 ^{o}C, and then vigorously stirring in an equal volume of ice-cooled sodium nitrite solution. Benzoylacetone in sodium hydroxide solution was been coupled with the cooled diazonium salt solution. Hydrochloric acid was been used to neutralize the reaction mixture, and the precipitate that resulted from that process was filtered off, washed with water, dried, and crystallized from ethanol to produce the matching azocoumarin color, scheme (1). Using IR spectra, the synthesized compound's characterization was established. IR (ν / Cm^{-1}), 3063 (-CH, arom.), 2981, 2927 (-CH, aliph), 1726 (-C=O), 1647 (-C=N).

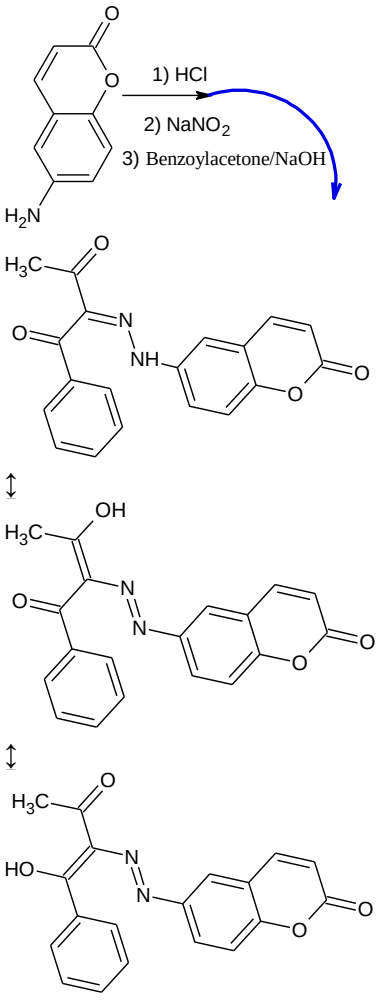

Scheme (1): The Synthesis and structure of the investigated compound and its possible tautomers

2.2. DFT calculations

In order to optimize the geometry of the subject compound, hybrid correlation functional (B3LYP) in conjunction with the basis sets 6-311 (d, p) were used [xi]. Quantum chemical properties have been calculated using the HOMO and LUMO energy values of the titled compound [xii].

2.3. Molecular docking Analysis

In order to determine the potential binding modes of the investigated compound against the breast cancer-specific DNA damage-binding protein (DDB1) receptor (PDB ID: 3I89), the RNA-dependent RNA polymerase (NS5B) of the Hepatitis C virus (HCV) (PDB ID: 5TRH), the core protein of the Hepatitis B virus (HBV) (PDB ID: 5T2P), and the crystal structure of the Fab fragment of an anti-Hepatitis A virus (HAV) antibody (PDB ID: 5WTG). The RCSB PDB database was been used to download the 3D protein structures. The named compound's improved structure served as the substrate.

3. Results and Discussion

3.1. DFT calculations

3.1.1. Optimized structures

Density functional theory (DFT) method based on B3LYP/6-311G (d, p) basis set was used to thoroughly optimize the 3D geometry of all potential tautomers of the molecule (L-T1, L-T2, and L-T3). Fig. (1) depicts the optimal structures of these tautomers.

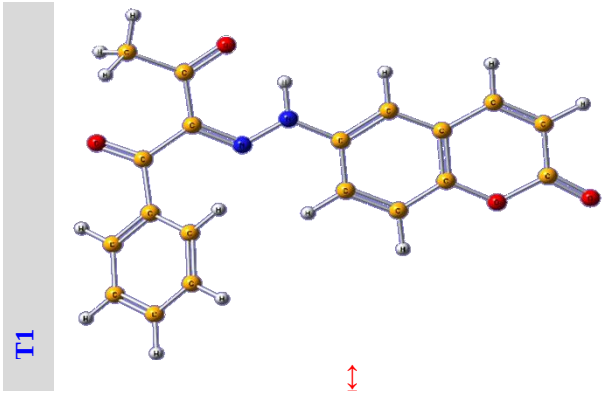

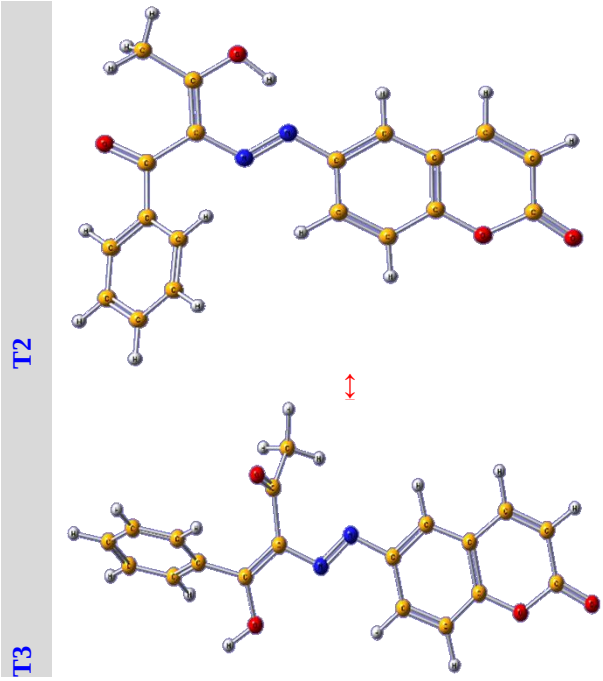

Fig. (1): Optimized structures of the possible tautomers of the titled compound

In solution media, these tautomers coexist, but only one of them is the most stable. Theoretically, the values of total energy (E_{Total}), enthalpy (H), and Gibbs free energy (G0) can be used to identify the tautomer that is the most stable, Table (1). The most stable structure was that of the tautomer with the lowest energy. L-T1 is the most stable tautomer as a result.

Table (1): Calculated thermo-chemical parameters (a.u.)

	L-T1	L-T2	L-T3
Total energy (E_{Total})	-31097.46	-31097.17	-31096.46
Enthalpy (H)	-31096.87	-31096.59	-31095.85
Gibbs free energy (G^0)	-31098.88	-31098.58	-31097.90

3.1.2. Spectroscopic investigation.

At the same theoretical level, the vibrational frequencies (FT-IR) of the most stable tautomer (L-T1) were determined and scaled down using scaling factor 0.961. The estimated vibrational frequencies and related experimental values were contrasted, Fig. (1.a). Important computed (experimental) vibrational frequencies (cm^{-1}) were found to be: 3180 (3070), 1756 (1726), and 1653 (1647), which, respectively, corresponded to ν(-NH), (-C=O), and (-C=N). Small variations were been discovered between calculated and experimental values. These variations result from various measured situations. Where the experimental data were recorded in solid phase while the theoretical values were derived in gaseous phase [xiii].

Linear correlation analysis was been performed using the computed frequencies and their experimental values, Fig. (1.b), which showed high linear correlation constant ($\mathbf{R^2}$), $\nu_{calculated} = 1.00\ \nu_{experimental} + 49.16$ ($R^2 = 0.997$). At the same level of theory, the electronic spectrum of the aforementioned molecule was theoretically estimated using the time-dependent density functional theory (TD-DFT) in gas phase. Fig (1.c) shows the comparison between the estimated electronic spectra and the matching experimental results. Table includes the estimated and measured wavelengths (λ_{max}, nm), excitation energies (E, eV), oscillator strength (*f*), and significant orbital contribution, Table (2). The calculated findings demonstrated that the first and second λ_{max} absorption bands in the TD-DFT UV-Vis spectra matched to the HOMO-7→LUMO+6 and HOMO-1→LUMO transitions, Fig. (1.c).

Table (2): Calculated and experimental electronic spectral data; wavelength (λ_{max}, nm), excitation energy (E, eV), oscillator strength (f) and major orbital contribution

Experimental λ_{max} (225 and 340 nm)				
TD-DFT	**λ_{max}**	**E, eV**	***f***	**Major Electronic transitions**
	391.25	3.1689	0.0180	HOMO-7 to LUMO+6
	257.24	4.8197	0.2948	HOMO-1 to LUMO

3.1.3. Charge distribution analysis

3.1.3.1. Molecular electrostatic potential (MEP) map

The docking of the substrate with the protein is significantly influenced by the existence of partial charges on both the substrate and the protein. Understanding the 3D structural and topological characteristics of the substrate can be done with the use of the molecular electrostatic potential (MEP) diagram. MEP identifies the molecular geometry point at which the influence of nuclei or electrons is predominant. Different hues, ranging from blue to red, were been used to represent different MEP diagram values. Electrophilic and nucleophilic reactivity are associated in the positive (blue) and negative (red) sections of the MEP, respectively. Regions of the surface that are negatively charged are depicted by the red colors (i.e., those areas where accepting an electrophile is most favorable). An increase in negative charge in a compound indicates the attraction of that chemical's appropriate sites in interactions with electrophiles. At the level of theory of the optimized shape, Molecular Electrostatic Potential (MEP) Diagram for the titled compound is mapped up, Fig (1.d). Due to their environment of abundant electrons, which makes them desirable targets for electrophilic attack, the majority of the negative areas (red) in the subject substrate are located around the carbonyl group of the coumarin moiety. In contrast, more positive areas (blue) are mostly directed toward the H-atom that may serve as an H-bond donor in intermolecular interactions between proteins and ligands Fig. (1.d).

3.1.3.2. Mulliken Population analysis

Due to their impact on dipole moment, polarizability, electronic structure, vibrational spectra, and other features for a molecule system, atomic charges play a significant role

in the application of quantum chemical calculations to molecular systems. The atoms' charge distributions point to the development of donor and acceptor pairs that would involve charge transfer in the molecule and regulate its ability to be both electrophilic and nucleophilic. Using the same level of theory, the Mulliken population analysis results for the subject molecule in gas phase were calculated and shown in Fig (1.e).

As a result, the carbonyl group of the coumarin moiety is where the majority of the negative charges are concentrated, which gives them their donor capacity. While hydrogen atoms had the highest positive atomic charges, Fig. (1.e).

(a)

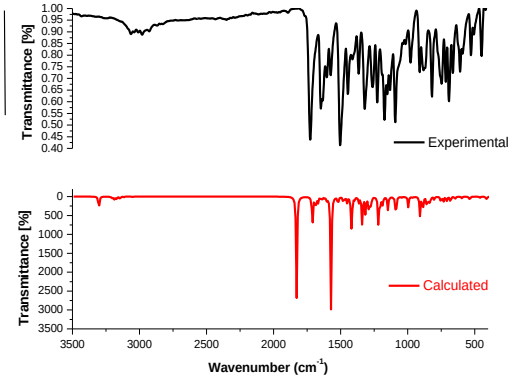

(b)

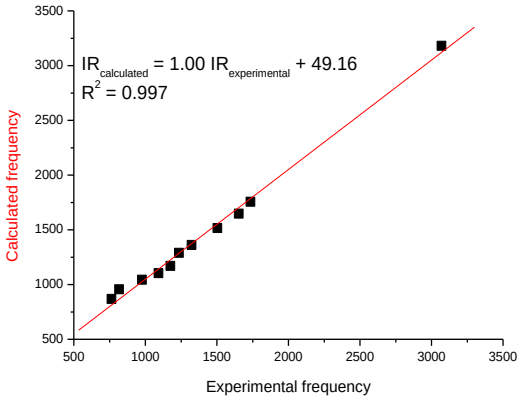

(c)

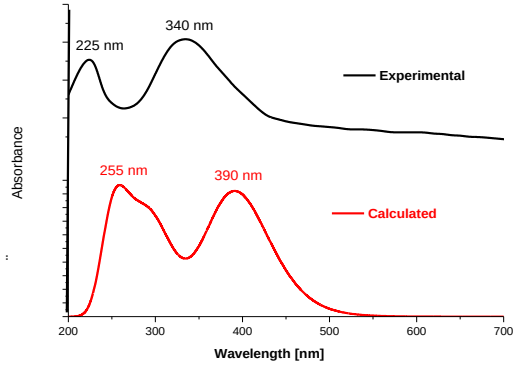

(d)

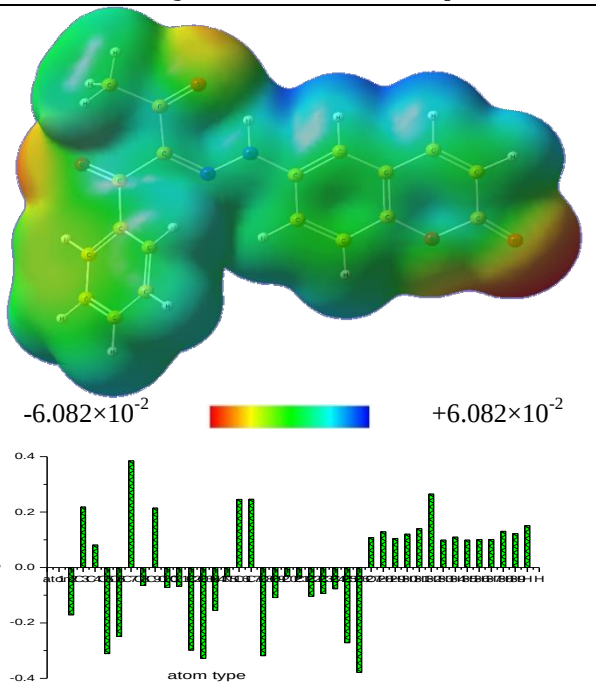

(e)

Fig. (1): **(a)**: Theoretical and calculated IR; **(b)**: Linear correlation of theoretical and calculated IR; **(c)**: Experimental-Calculated UV-vis.; **(d)**: Molecular electrostatic potential (MEP) of the titled compound, **(e):** Mulliken Population analysis .

3.1.4. Reactivity descriptors

3.1.4.1. Frontier molecular orbital's (FMOs)

The frontier orbital (FMO), highest occupied molecular orbital (HOMO), and lowest unoccupied molecular orbital (LUMO), characterise the chemical reactivity and kinetic stability of the molecule and control how it interacts with other species. The orbitals known as HOMO and LUMO serve largely as electron donors and acceptors, respectively. Fig. (2) shows the HOMO and LUMO energies as well as contour diagrams for the chemical in question. It is evident that the HOMO and LUMO orbitals on the Chromene moiety of the named compounds are delocalized.

L

LUMO

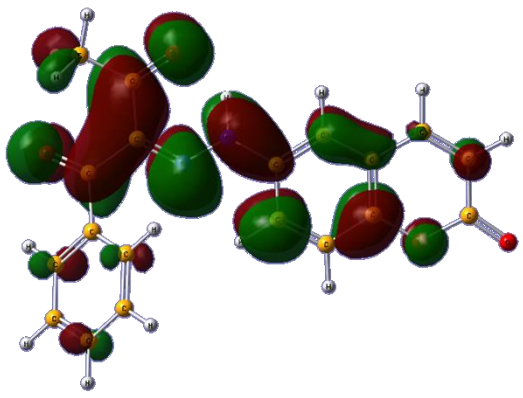

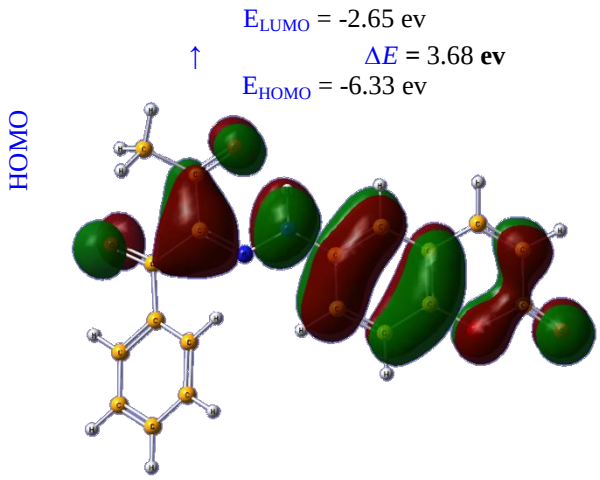

Fig. (2): The contour diagrams of FMOs of the titled compound

3.1.4.2. Global reactivity descriptors

The term "HOMO" denotes the ability of a nucleophile to donate an electron, and the energy of the HOMO is directly related to the ionization potential (I= -E_{HOMO}). The electrontrophile tendency is implied by the LUMO value, and the LUMO energy is directly related to the electron affinity (A=-E_{LUMO}).

Selected global quantum chemical descriptors, including energy gap (ΔE), electronegativity (χ), electronic chemical potential (CP), global chemical hardness (η), global softness (σ), global electrophilicity index (ω), electronic charge (N_{max}), and nucleophilicity index (Nu), were calculated using ionisation potential (I) and electron affinity (A) [xiv,xv,xvi,xvii], Table (3). Significantly predicting the compound's biological activity are these quantum chemical characteristics.

Table (3): Global chemical reactivity descriptors, E_{HOMO}, E_{LUMO}, energy gap (ΔE), ionization potential (I), electron affinity (A), electronegativity (χ), chemical hardness (η), softness (σ), chemical potentials (μ), electrophilicity index (ω), and nucleophilicity (Nu) of the titled compound.

	E_{HOMO}	E_{LUMO}	ΔE	I	A	
L	-6.33	-2.65	3.68	6.33	2.65	
	χ	μ	η	σ	ω	Nu
	4.49	-4.49	1.84	0.27	5.48	0.18

3.2. Molecular docking

Before being used in actual applications, the synthesized substrate was docked against the receptors of the crystal structures of breast cancer (PDB ID: 3I89), HCV (PDB ID: 5TRH), HBV (PDB ID: 5T2P), and HAV (PDB ID: 5WTG). Fig. (3) depicted the target receptors' three-dimensional structure as well as the active site pocket with the Dummy atoms where molecule docking took place. Table (4) summarizes the molecular docking outcome.

It's interesting to note that the subject substrate has strong negative docking scores and forms numerous hydrogen bonds and hydrophobic interactions with all of the target receptors (S), Fig. (4) and Table (4). That shows the docked substrate's robust contact with the receptor's active site. The hydrophobic property of the subject substrate would make it easier for them to play their part in inhibiting the target HCV, HBV, and HAV receptors by blocking their active site [xviii,xix].

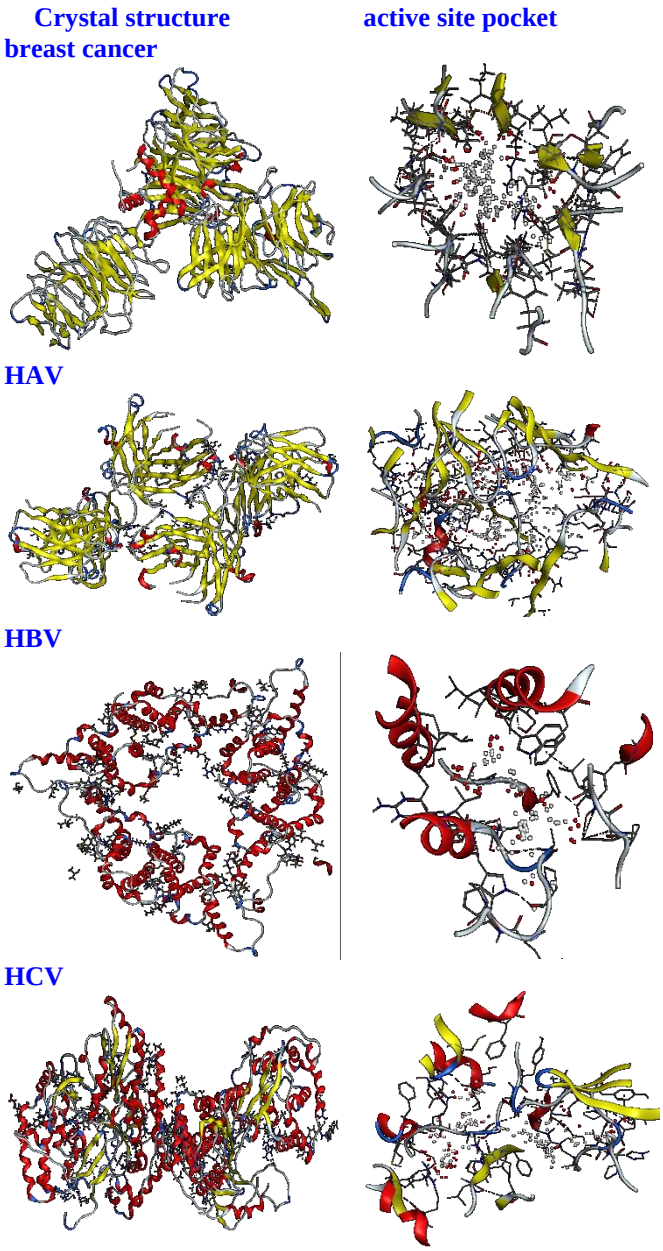

Fig. (3): the crystal structure, active site pocket of **breast cancer** (3I89)**, HCV** (5TRH), **HBV** (5T2P) and **HAV** (5WTG).

Table (4): Docking results, and Amino acid residues-titled compound interactions, obtained through docking of the studied compounds with crystal structure of **breast cancer** (3I89)**, HCV** (5TRH), **HBV** (5T2P) and **HAV** (5WTG).

Substrate site	Receptor site	Interaction	Distance (Å)	E (kcal/mol)	S (kcal mol^{-1})
Breast					
N 12	PHE 458	H-donor	3.05	-1.50	-5.92
O 11	ARG 589	H-acceptor	3.29	-1.70	
6-ring	LYS 408	pi-H	4.37	-0.60	
6-ring	TYR 678	pi-H	4.18	-0.60	
HAV					
N 12	GLN 164	H-donor	3.47	-1.00	-6.33
6-ring	LYS 38	pi-cation	4.71	-2.50	
HBV					
6-ring	LEU 140	pi-H	4.48	-2.20	-8.01
6-ring	LEU 140	pi-H	4.19	-0.80	
6-ring	LEU 140	pi-H	4.18	-0.60	
HCV					
O 11	ARG 48	H-acceptor	3.03	-4.40	-6.32
O 17	SER 556	H-acceptor	3.09	-1.10	
6-ring	LEU 159	pi-H	3.91	-3.10	

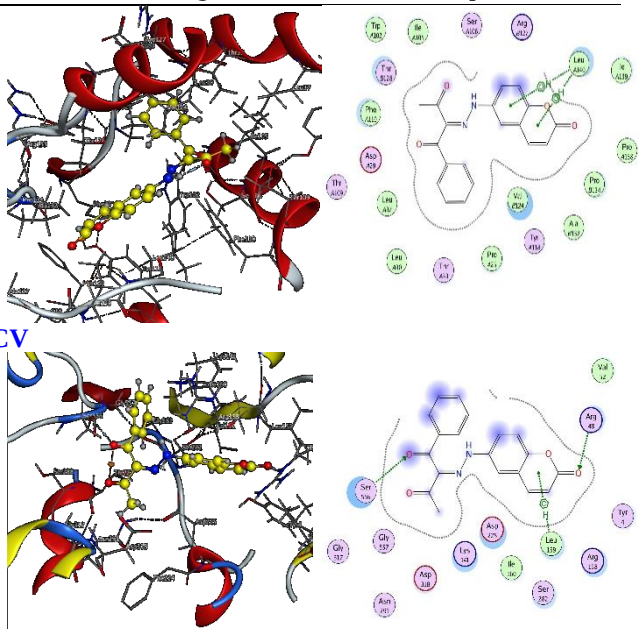

Fig. (4): 2D and 3D orientation of the best pose of the titled compound in the active site pocket of **breast cancer** (3I89)**,** **HCV** (5TRH), **HBV** (5T2P) and **HAV** (5WTG).

HBV was the most inhibited disease by the named substance, followed by HAV, HCV, and breast cancer. The named compound is therefore the most effective against HBV**,** Fig. (5). Through the integration of a variety of strong hydrogen bonds and hydrophobic interactions, this molecule successfully attached to the substrate binding pocket. As a result, it has the potential to be an effective antiviral candidate.

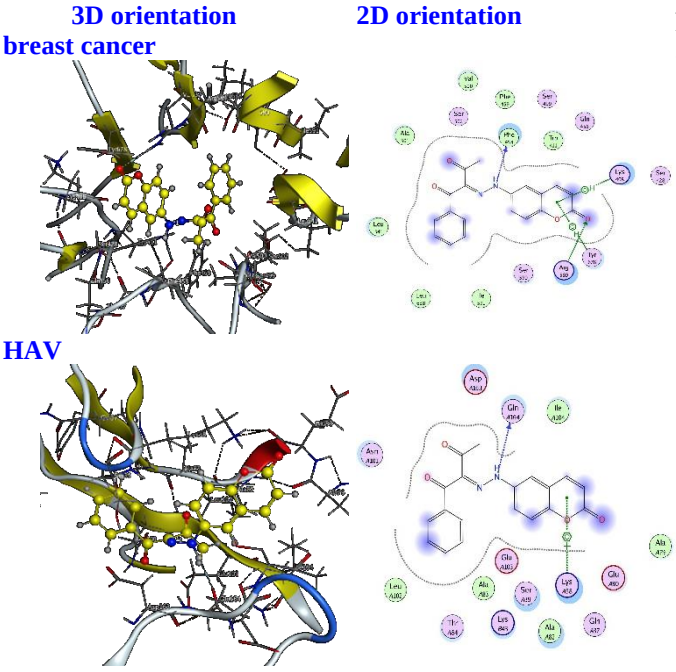

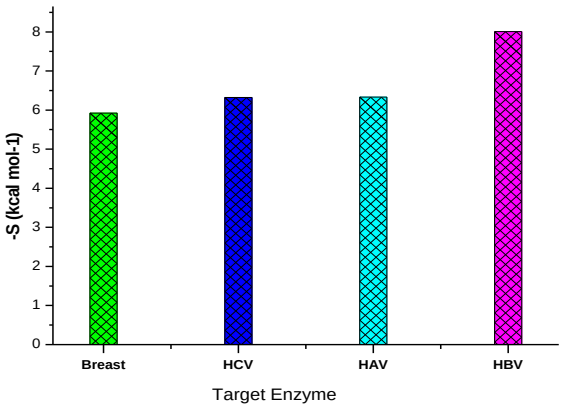

Fig. (5): Histogram of the binding energy (**-S**, kcal/mol) between titled compound with different protein receptors**.**

Conclusion

The structural geometry, spectroscopic characteristics, and

reactivity parameters of the synthesised (2E)-1-phenyl-butane-1,2,3-trione 2-[(2-oxo-2H-chromene-6-yl)hydrazone were obtained in this work using the DFT/B3LYP technique. The estimated vibrational and electronic spectra and the matching experimental values were in good agreement. The docking of the synthesised ligand to the crystal structures of breast cancer (3I89), HCV (5TRH), HBV (5T2P), and HAV (5WTG) provided an initial understanding of the interaction with the protein's active site. The title substance has the maximum binding activity to HBV, according to docking data.

References

[i] Kamel, M. S.; Belal, A.; Aboelez, M. O.; Shokr, E. K.; Abdel-Ghany, H.; Mansour, H. S.; Shawky, A. M.; El-Remaily, M. A. E .A .A. A. Molecules 2022, 27, 2061. https://doi.org/10.3390/molecules27072061

[i] Antar A. Abdelhamid, Kaoud S. M. Salama, Ahmed M. Elsayed, Mohamed A. Gad, and Mahmoud Abd El Aleem Ali Ali El-Remaily, ACS Omega 2022, 7, 5, 3990–4000, https://doi.org/10.1021/acsomega.1c05049

[i]Qamar, M.T. ul, Saleem, S., Ashfaq, U. A., Bari, A., Anwar, F., Alqahtani, J. Transl. Med., 17 (362) (**2019**), 1-14.

[i] Francesca Annunziata, Cecilia Pinna, Sabrina Dallavalle, Lucia Tamborini1, Andrea Pinto, Int. J. Mol. Sci. 21 (**2020)** 4618

[i] Borges, F.; Roleira, F.; Milhanzes, N.; Santana, L.; Uriarte, E., Curr. Med. Chem.2005,12, 887–916

[i] Kummerle, A.E.; Vitorio, F.; Franco, D.P.; Pereira, T.M., Curr. Top. Med. Chem.2018,18, 124–128

[i] T. Tahir, M. Ashfaq, H. Asghar, M.I. Shahzad, R. Tabassum, A. Ashfaq, Mini Rev. Med. Chem., 18 (0) (**2018**) 1-13.

[i] E. Török, E. Moran, F. Cooke, Oxford Handbook of Infectious Diseases and Microbiology**,** Oxford University Press, Oxford (**2009**), p. 56

[i] Aly Abdou, Hassan M. Mostafa, Abdel-Mawgoud M. Abdel-Mawgoud, Inorganica Chimica Acta, 539, **2022**, 121043, https://doi.org/10.1016/j.ica.2022.121043

[i] Abdel-Megied, F. M. E., El-Kaschef, M. A. F., and Ghaas, A. A. G., Egypt J. Chem. 20, 433 (1077).

[i] M.J. Frisch, G.W. Trucks, H.B. Schlegel, G.E. Scuseria, M.A. Robb, J.R. Cheeseman, et al., Gaussian 03, Revision of C.01, Gaussian Inc., Wallingford CT (2004

[i] A. Abdou, O.A. Omran, A. Nafady, I.S. Antipin, Arab. J. Chem., 15 (3) (2022), Article 103656, 10.1016/j.arabjc.2021.103656

[i] Salah M. A. Ridha, Zeyad A. Saleh, Firyal Weli Askar, Physical Chemistry, 5 (**2015**) 6-15

[i] Aly Abdou, Hassan M. Mostafa, Abdel-Mawgoud M. Abdel-Mawgoud, Inorganica Chimica Acta, 539 (**2022**) 121043, https://doi.org/10.1016/j.ica.2022.121043.

[i] Aly Abdou, Journal of Molecular Structure, Volume 1262, **2022**, 132911, https://doi.org/10.1016/j.molstruc.2022.132911

[i] Nadia A. A. Elkanzi, Ali M. Ali, Hajer Hrichi, Aly Abdou, Appl Organomet Chem **2022**, 36(5), e6665. https://doi.org/10.1002/aoc.6665.

[]i A . Th amarai, R . V ad amalar, M.Raja, S. Muthu, B. Narayana, P. Ramesh, R. Raj Muhamed, S. Sevvanthi, S. Aayisha, Spectrochimica Acta Part A: Molecular and Biomolecular Spectroscopy 226 (**2020**) 117609

[i] Aly Abdou, Abdel-Mawgoud M. Abdel-Mawgoud, Appl Organomet Chem **2022**, 36 (4), e6600. https://doi.org/10.1002/aoc.6600.

[i] Aly Abdou, Omran A. Omran, Ayman Nafady, Igor S. Antipin, Arabian Journal of Chemistry, Volume 15, Issue 3, **2022**, 103656, https://doi.org/10.1016/j.arabjc.2021.103656.